

Supporting Information for

Designing rock-salt-phase-enriched surface in Mn-based partially disordered spinel cathode materials to mitigate degradation in Li-ion batteries

Hyoj Jo,^{‡a} Changju Lee,^{‡a} HyeongJun Nam,^a Jee Ho Ha,^a Nyung Joo Kong,^a Kyojin Ku,^b Seok Ju Kang,^a and Sung-Kyun Jung^{*a}

Affiliation

a. Department of Energy Engineering, School of Energy and Chemical Engineering, Ulsan National Institute of Science and Technology (UNIST), Ulsan 44919, Republic of Korea

b. Department of Materials Science and Engineering, Hanbat National University, N8-316, 125 Dongseodaero, Yuseong-gu, 34158, Daejeon, Republic of Korea

* Corresponding to: skjung@unist.ac.kr

‡ These authors contributed equally to this work.

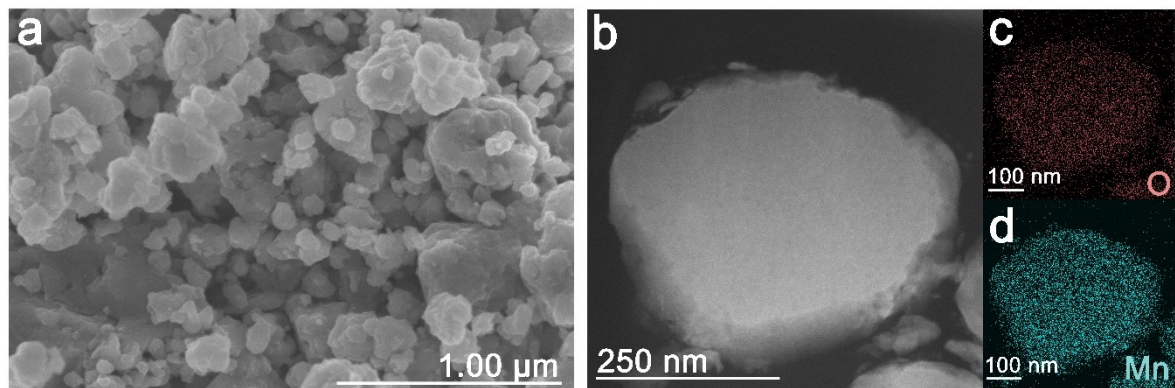


Fig. S1 (a) SEM image and (b) TEM image of pristine $\text{Li}_{1.33}\text{Mn}_2\text{O}_4$ and (c, d) corresponding O (red) and Mn (blue) maps of the particle region.

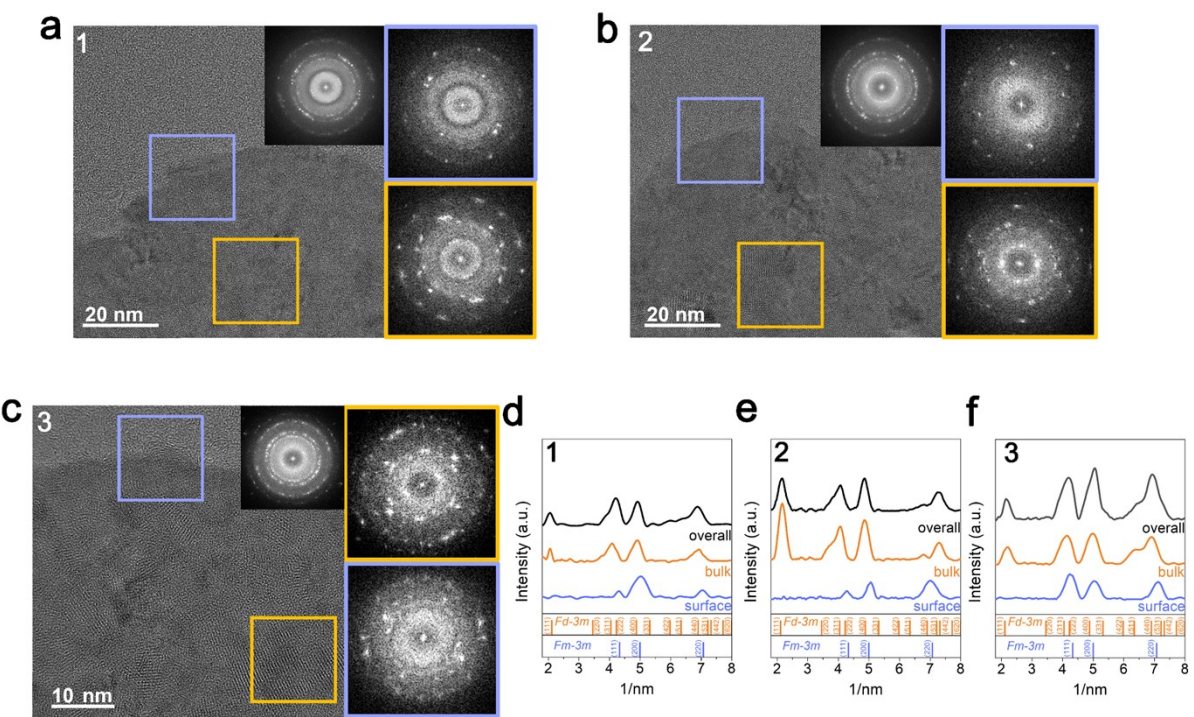


Fig. S2 (a–c) TEM images and FFT patterns of various regions of $\text{Li}_{1.33}\text{Mn}_2\text{O}_4$. The yellow and blue boxes at different local positions are dominated by spinel-like and DRX-like phases, respectively. (d–f) Azimuthal integration patterns of FFT for surface, bulk, and overall images in the TEM image of the same number.

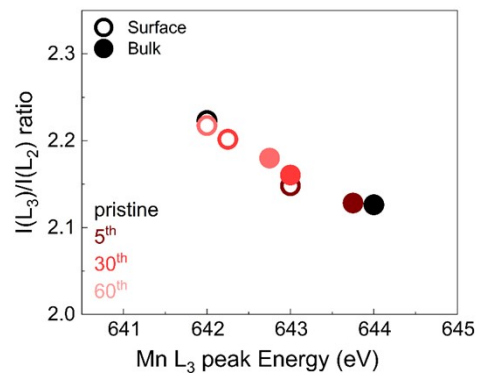


Fig. S3 L_3/L_2 ratio obtained from EELS spectra of $Mn\ L_{3,2}$ -edge for surface (open circles) and bulk (solid circles) at various cycles (Fig. 4k): pristine, 5th, 30th, and 60th.

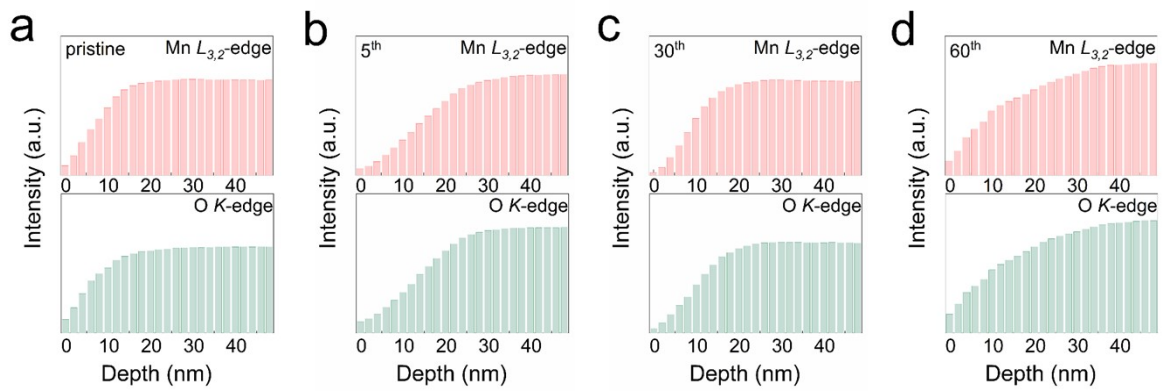


Fig. S4 Intensity profiles obtained by integrating elemental mapping images acquired from Mn- $L_{3,2}$ and O-K edge signals for various cycles. The intensity profile at each depth represents the average of the values measured in various local regions of the particle.

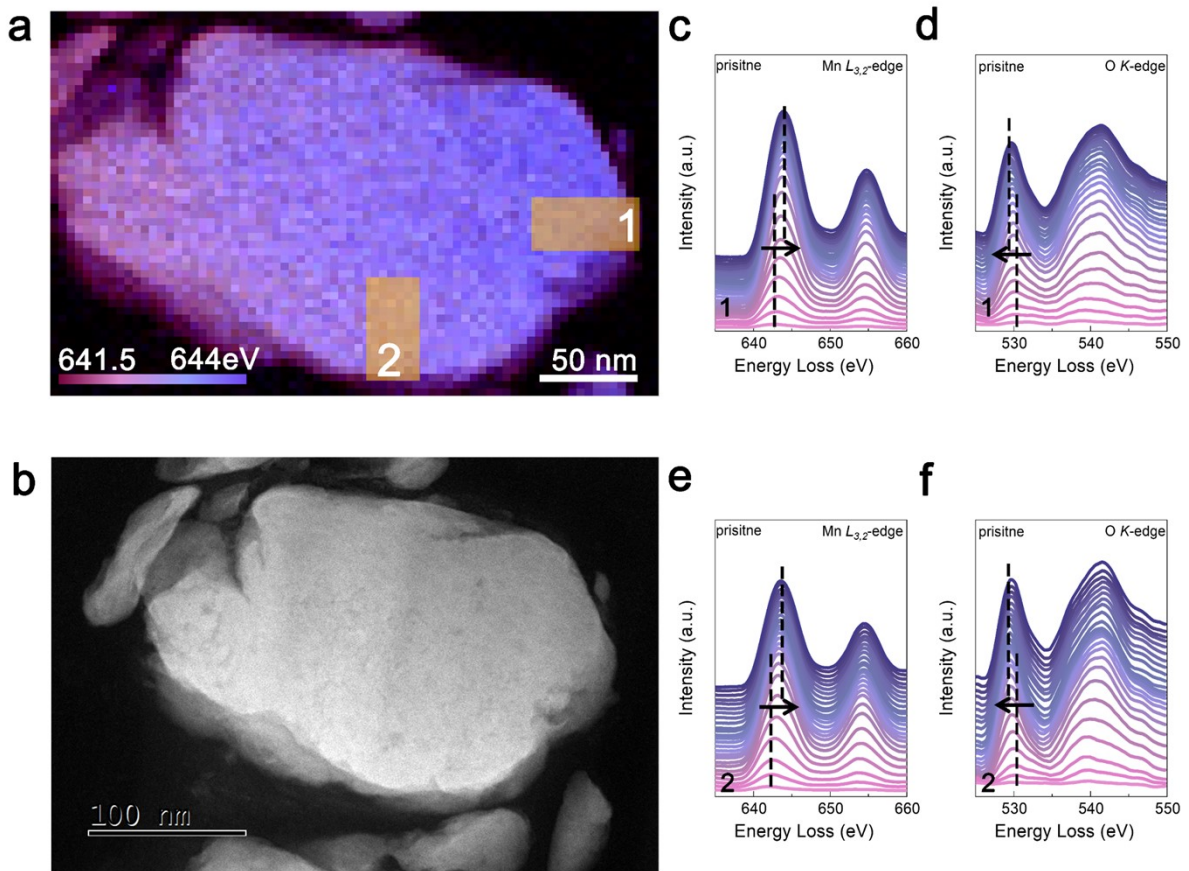


Fig. S5 (a) STEM-EELS images of pristine state for the energy distribution of the Mn $L_{3,2}$ -edge peak. (b) Annular dark field (ADF) image of the pristine state sampled by FIB. EELS spectra of (c, e) Mn $L_{3,2}$ -edge and (d, f) O K-edge peak from surface to bulk in the yellow boxes. (c,d) and (e,f) are spectra for yellow boxes no. 1 and no. 2, respectively.

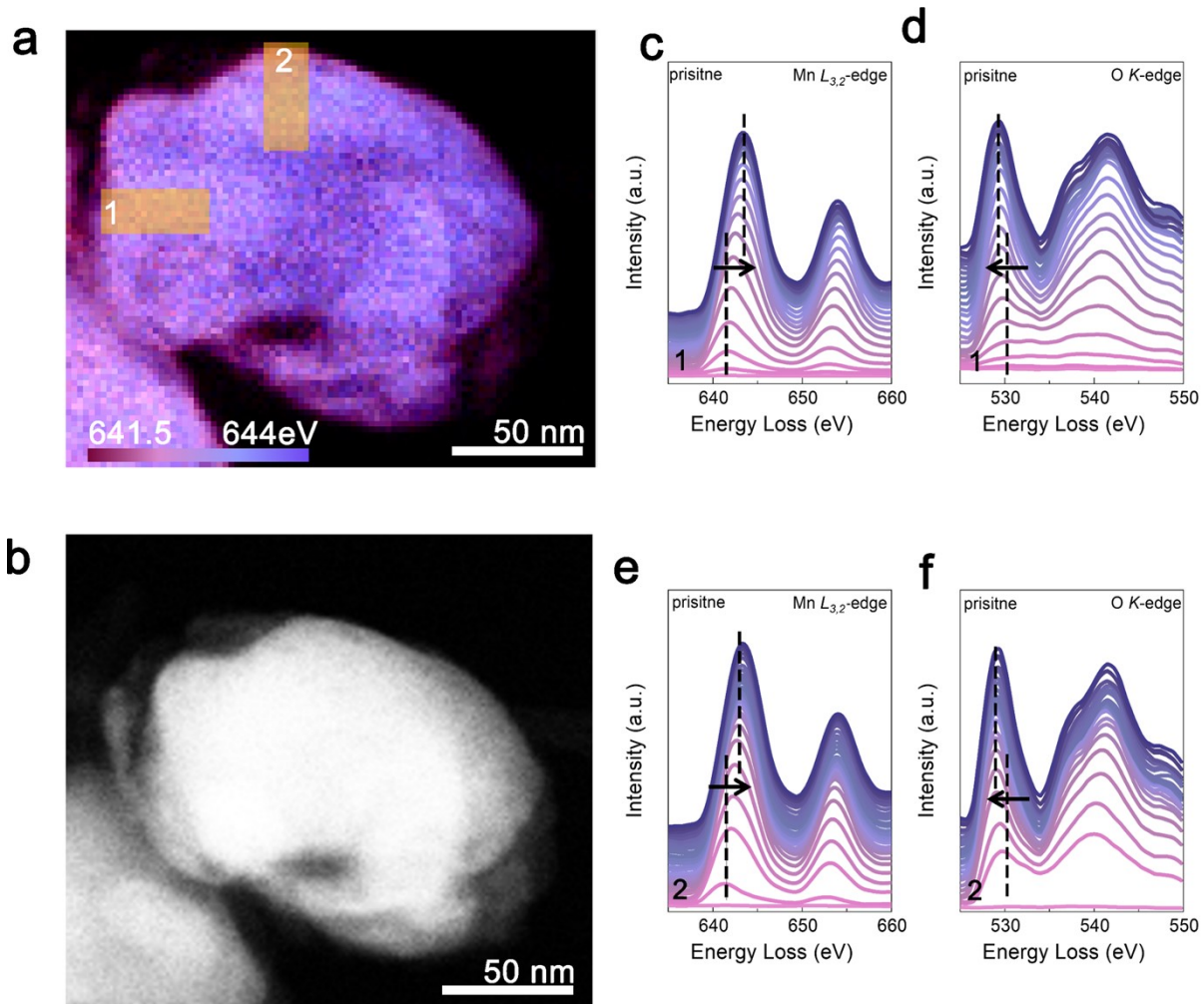


Fig. S6 (a) STEM–EELS images of pristine state for the energy distribution of the Mn $L_{3,2}$ -edge peak. (d) ADF image of the pristine state. EELS spectra of (c, e) Mn $L_{3,2}$ -edge peak and (d, f) O K-edge peak from the surface to the bulk in the yellow boxes. (c,d) and (e,f) are spectra for yellow boxes no. 1 and no. 2, respectively.

In TEM analysis, variations in the sample thickness can result in apparent differences between the surface and bulk characteristics due to edge effects. Therefore, we conducted analyses on both FIB-treated and non-FIB-treated $\text{Li}_{1.33}\text{Mn}_2\text{O}_4$. As shown in Fig. S5 and Fig. S6, regardless of the FIB treatment, differences in the spectra for Mn $L_{3,2}$ -edge and O K-edge between the surface and bulk were observed. Based on these observations, the differences between the surface and bulk were attributed to structural disparities.

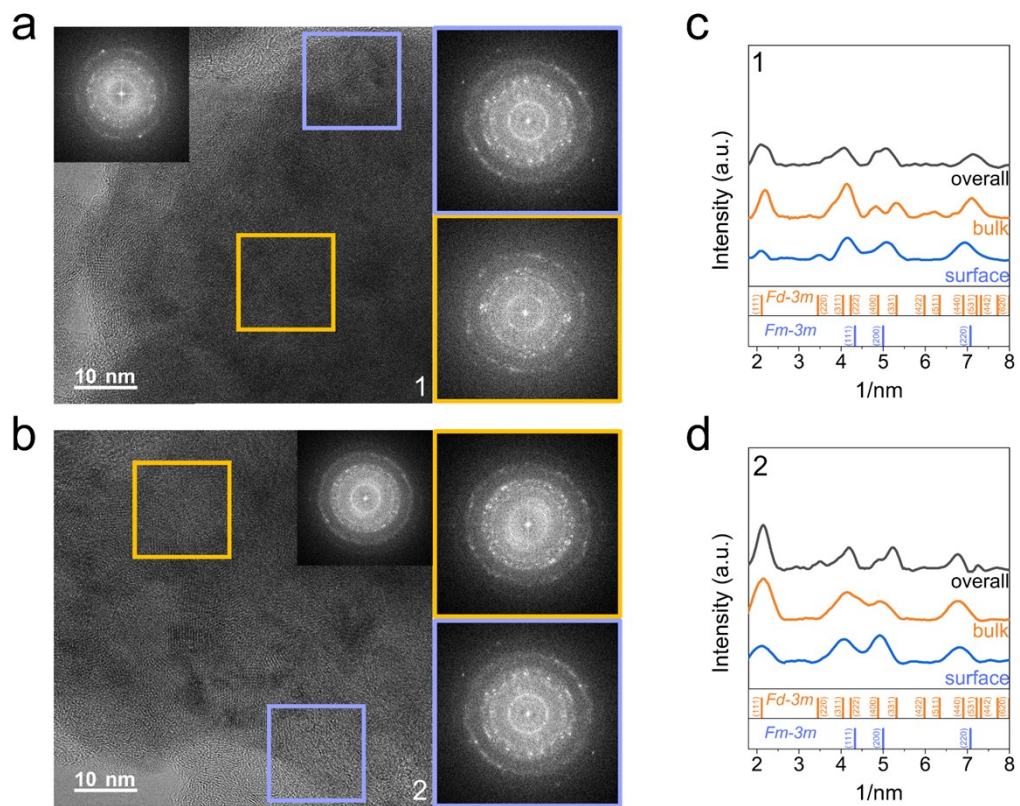


Fig. S7 (a,b) TEM images and FFT patterns of various regions at 2.85-V discharge state of 5th cycle. The yellow and blue boxes at different local positions are dominated by spinel-like and DRX-like phases, respectively. (c,d) Azimuthal integration patterns of FFT for surface, bulk, and overall images in the TEM image of the same number.

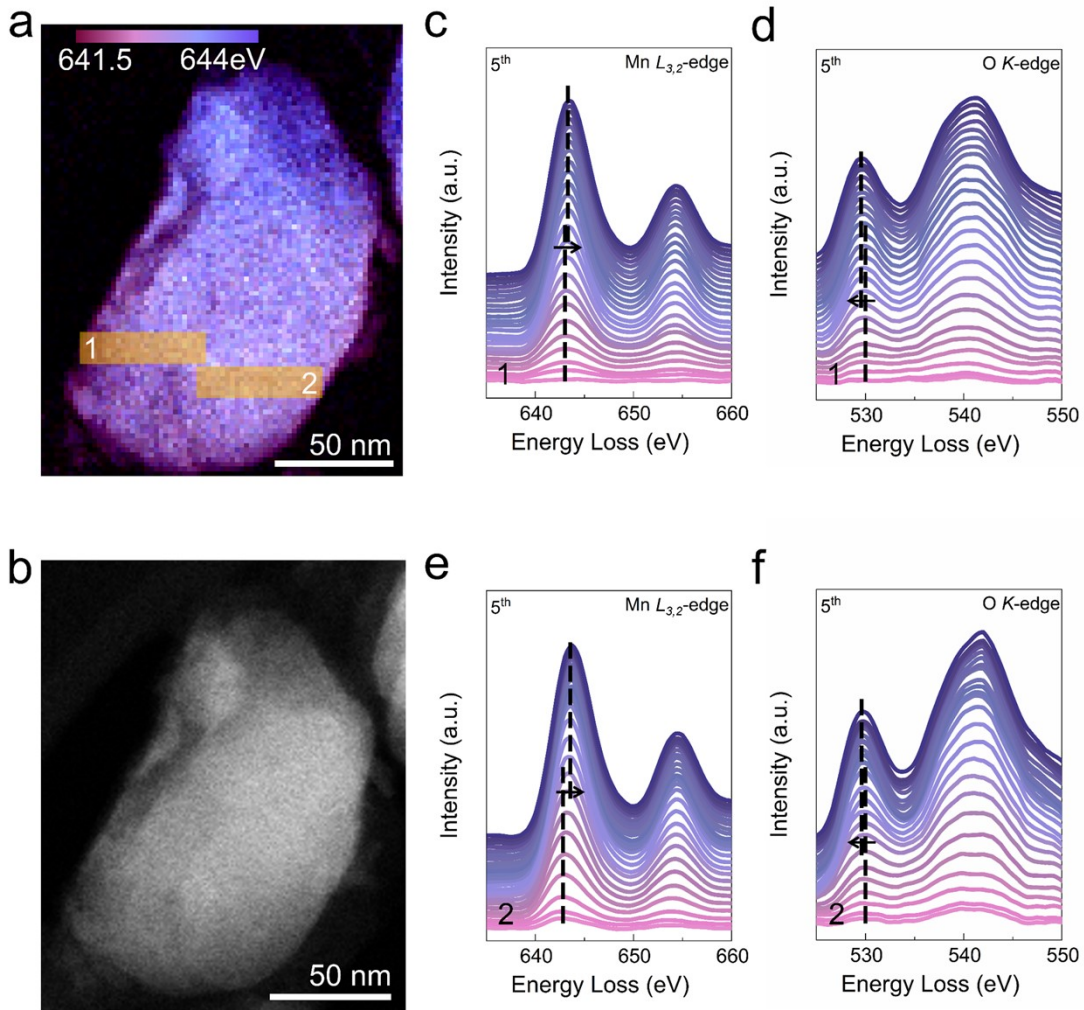


Fig. S8 (a) STEM–EELS images of the 5th cycle for the energy distribution of the Mn $L_{3,2}$ -edge peak. (b) ADF TEM image of the 5th cycle. EELS spectra of (c, e) Mn $L_{3,2}$ -edge peak and (d, f) O K-edge peak from the surface to bulk in the yellow boxes. (c,d) and (e,f) are spectra for yellow boxes no. 1 and no. 2, respectively.

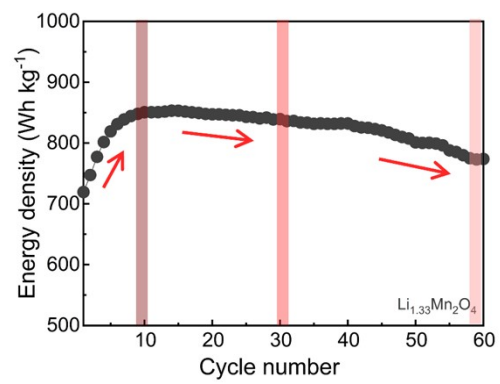


Fig. S9 The energy density of $\text{Li}_{1.33}\text{Mn}_2\text{O}_4$ upon increasing cycle numbers.

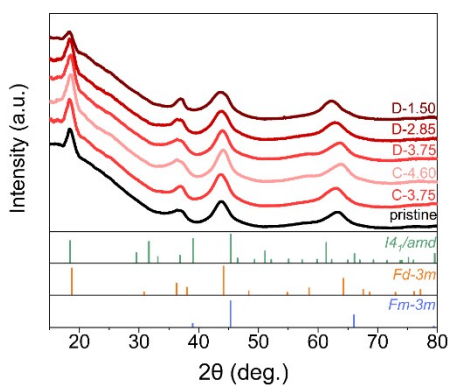


Fig. S10 *Ex-situ* XRD patterns of $\text{Li}_{1.33}\text{Mn}_2\text{O}_4$ electrode throughout first charge and discharge.

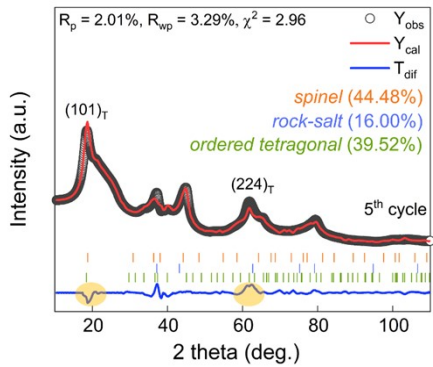


Fig. S11 Rietveld refinement of XRD data ($\lambda = 1.5406 \text{ \AA}$) for the electrode in the 5th discharge state, performed on the ordered tetragonal phase.

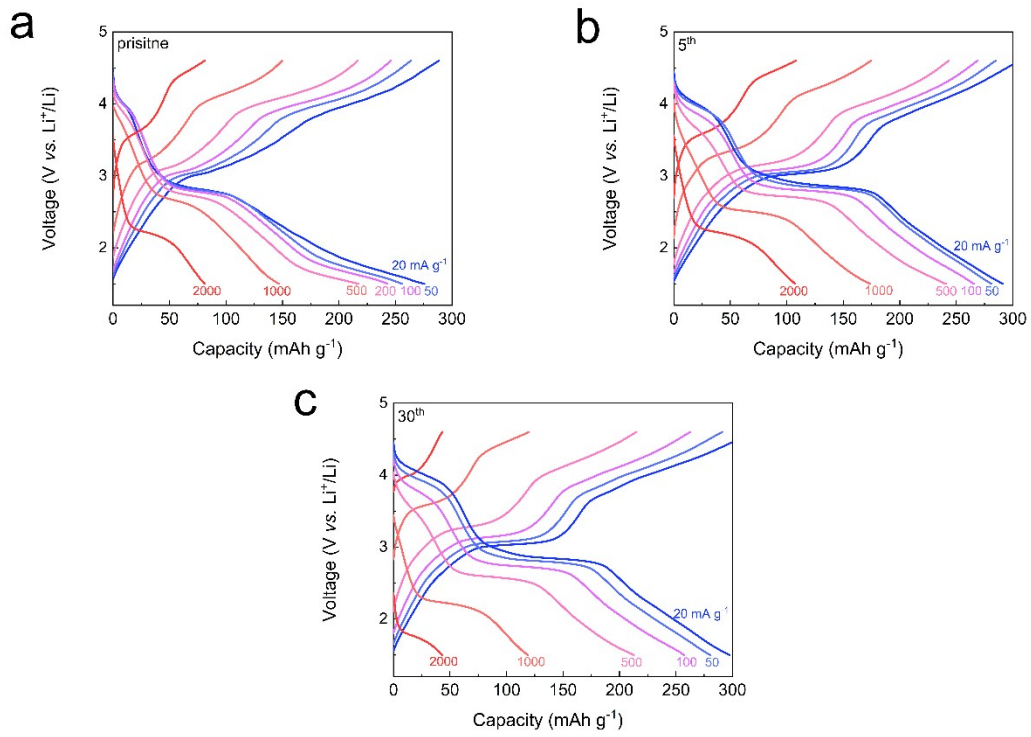


Fig. S12 Voltage profiles for various current densities for the pristine electrode and after the 5th and 30th cycles (60 °C, 50 mA g⁻¹).

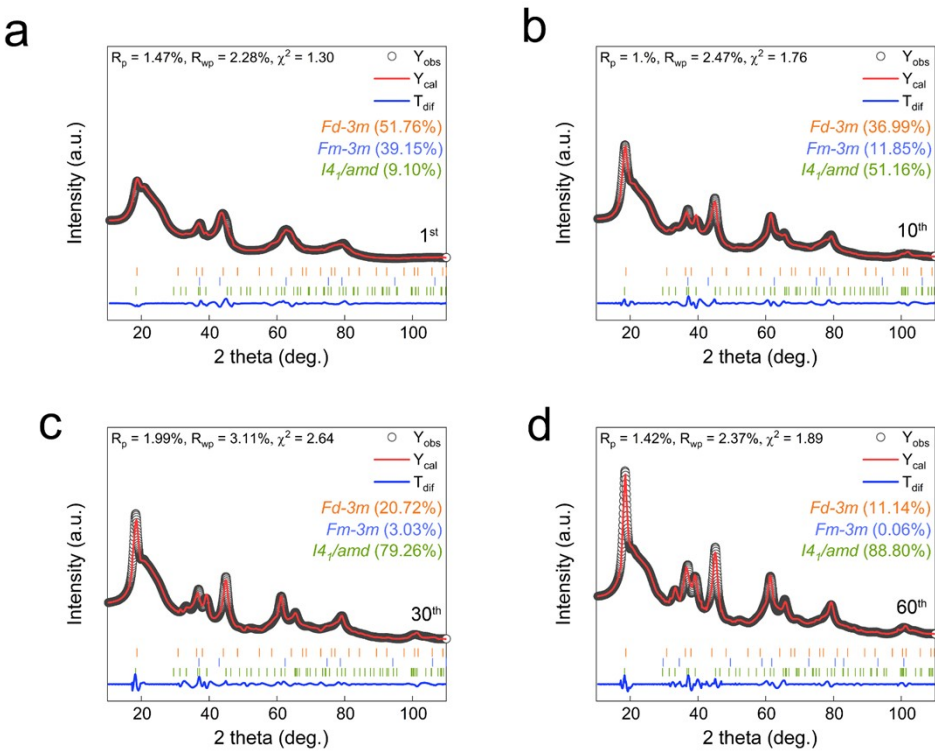


Fig. S13 Rietveld refinement of the XRD data ($\lambda = 1.5406 \text{ \AA}$) for the electrode in the discharged state after the (a) 1st, (b) 10th, (c) 30th, and (d) 60th cycle.

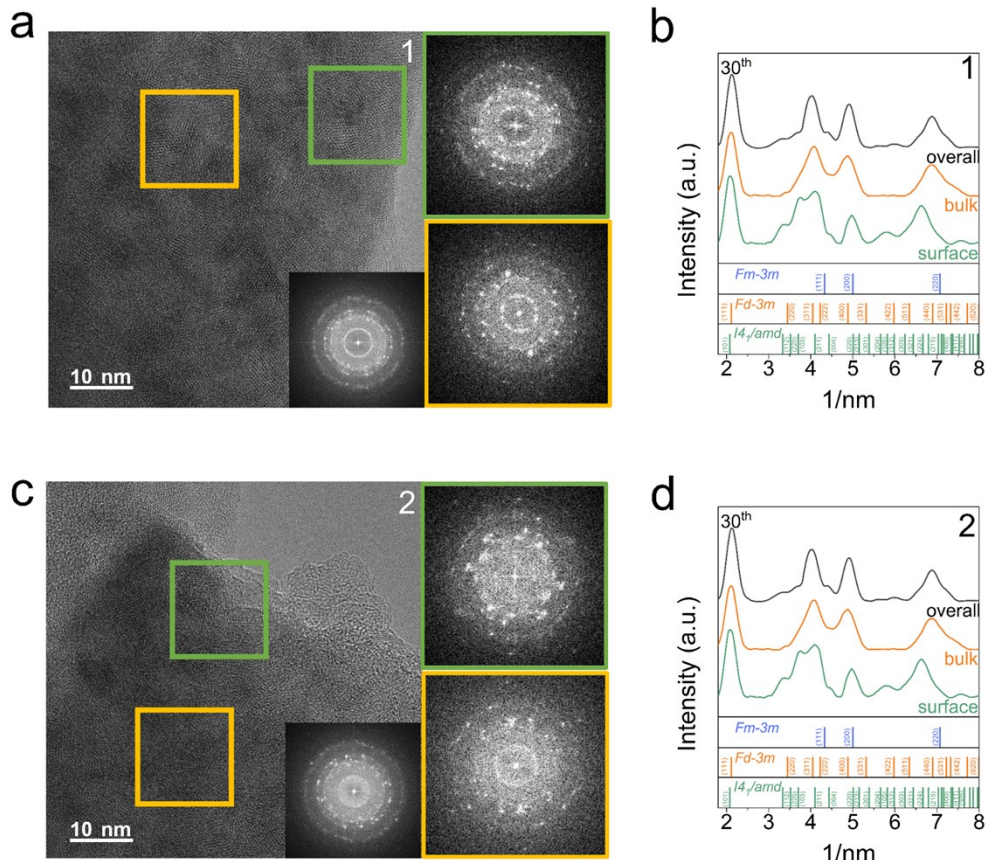


Fig. S14 (a,b) TEM images and FFT patterns of various regions at 2.85-V discharged state of 30th cycle. The regions within the yellow and green boxes at different local positions are dominated by spinel-like and tetragonal-like phases, respectively. (c,d) Azimuthal integration patterns of FFT for surface, bulk, and overall images in the TEM image of the same number.

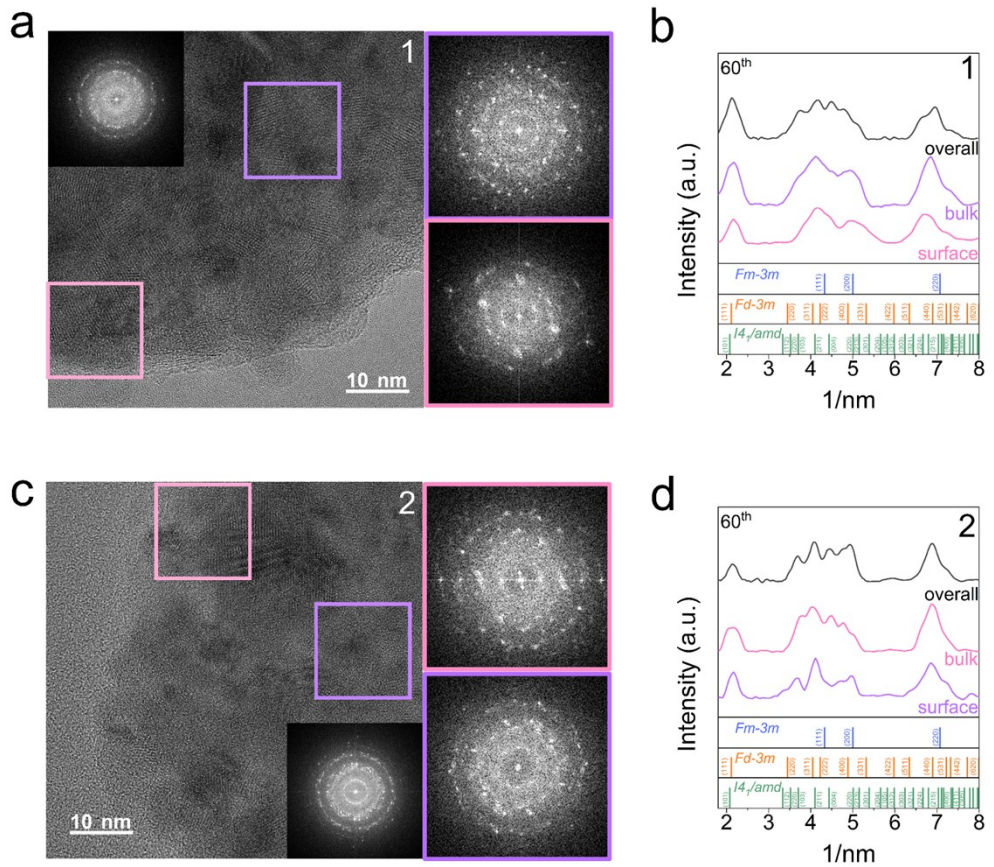


Fig. S15 (a,b) TEM images and FFT patterns of various regions at 2.85-V discharged state of 30th cycle. The areas within the pink and purple boxes at different local positions correspond to surface and bulk regions, respectively. (c,d) Azimuthal integration patterns of FFT for surface, bulk, and overall images in the TEM image of the same number.

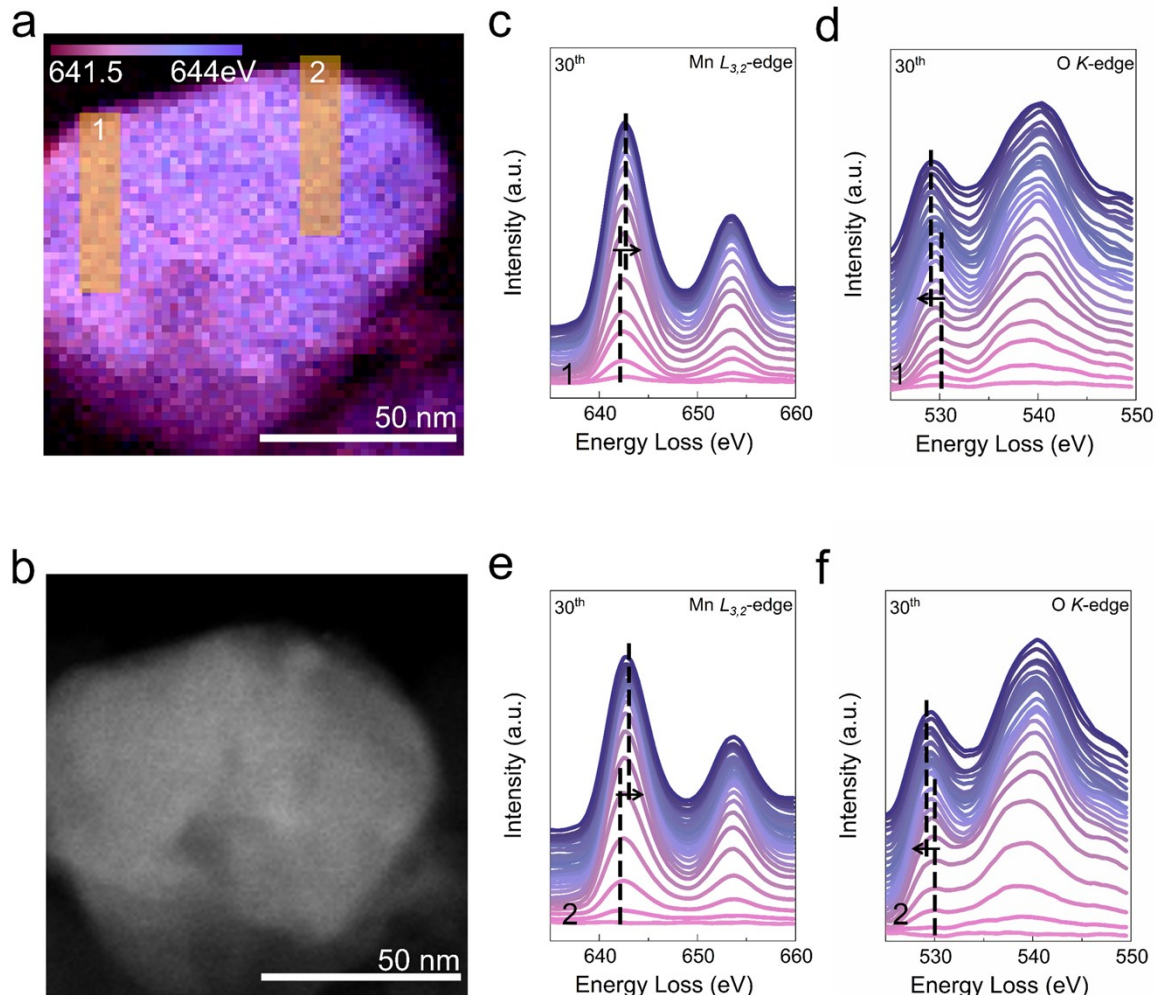


Fig. S16 (a) STEM-EELS images of the 30th cycle for the energy distribution of the Mn $L_{3,2}$ -edge peak. (b) ADF TEM image of 30th cycle. EELS spectra of (c, e) Mn $L_{3,2}$ -edge peak and (d, f) O K-edge peak from the surface to bulk in the yellow boxes. (c,d) and (e,f) are spectra for yellow boxes no. 1 and no. 2, respectively.

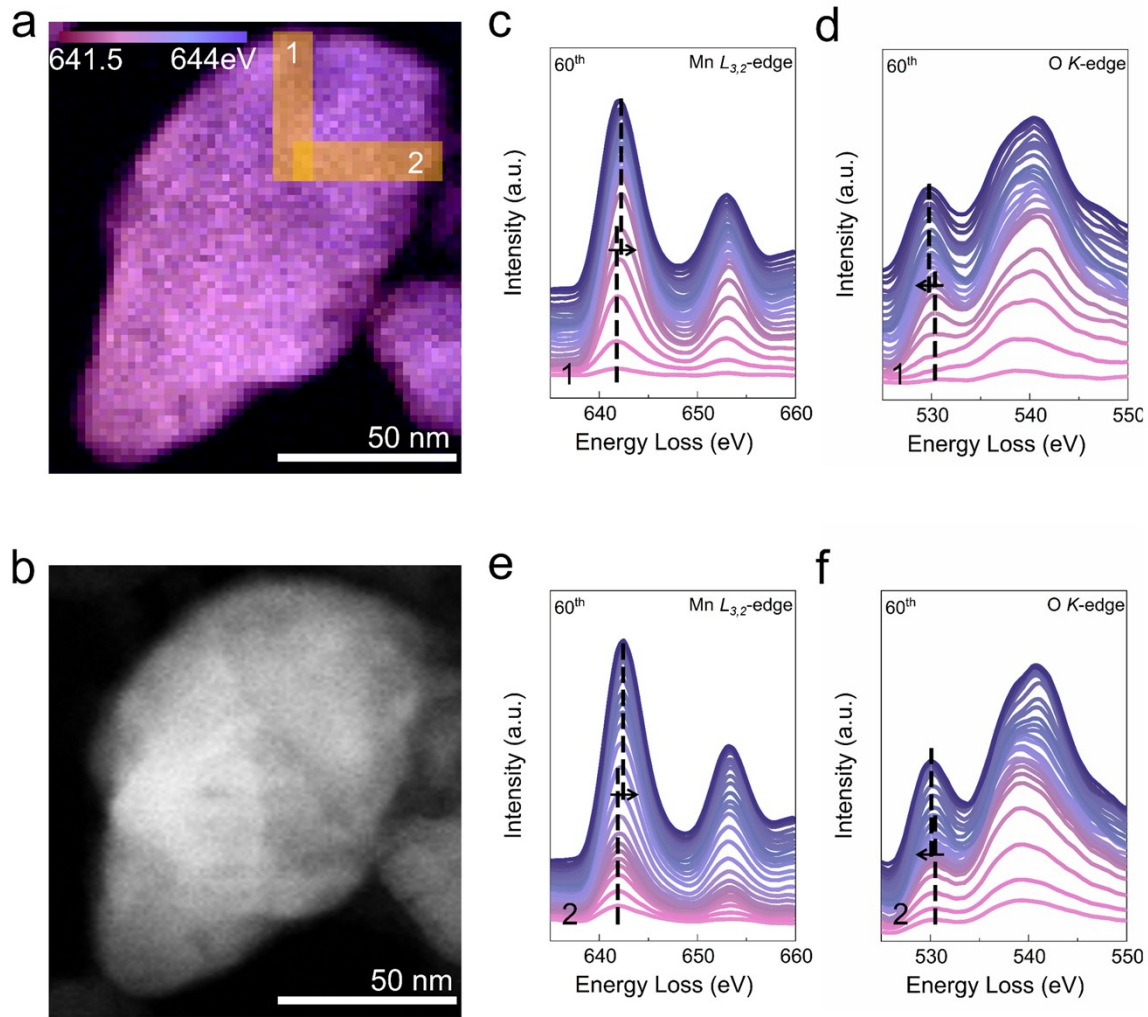


Fig. S17 (a) STEM-EELS images of the 60th cycle for the energy distribution of the Mn $L_{3,2}$ -edge peak. (b) ADF TEM image of 60th cycle. EELS spectra of (c, e) Mn $L_{3,2}$ -edge peak and (d, f) O K-edge peak from the surface to bulk in the yellow box. (c,d) and (e,f) are spectra for yellow boxes no. 1 and no. 2, respectively.

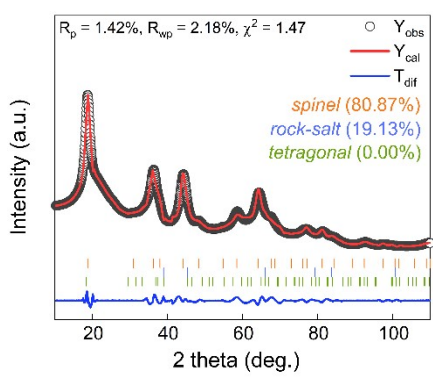


Fig. S18 Rietveld refinement of the XRD data ($\lambda = 1.5406 \text{ \AA}$) of nanocomposite $\text{Li}_{1.26}\text{Mn}_{1.88}\text{O}_4$.

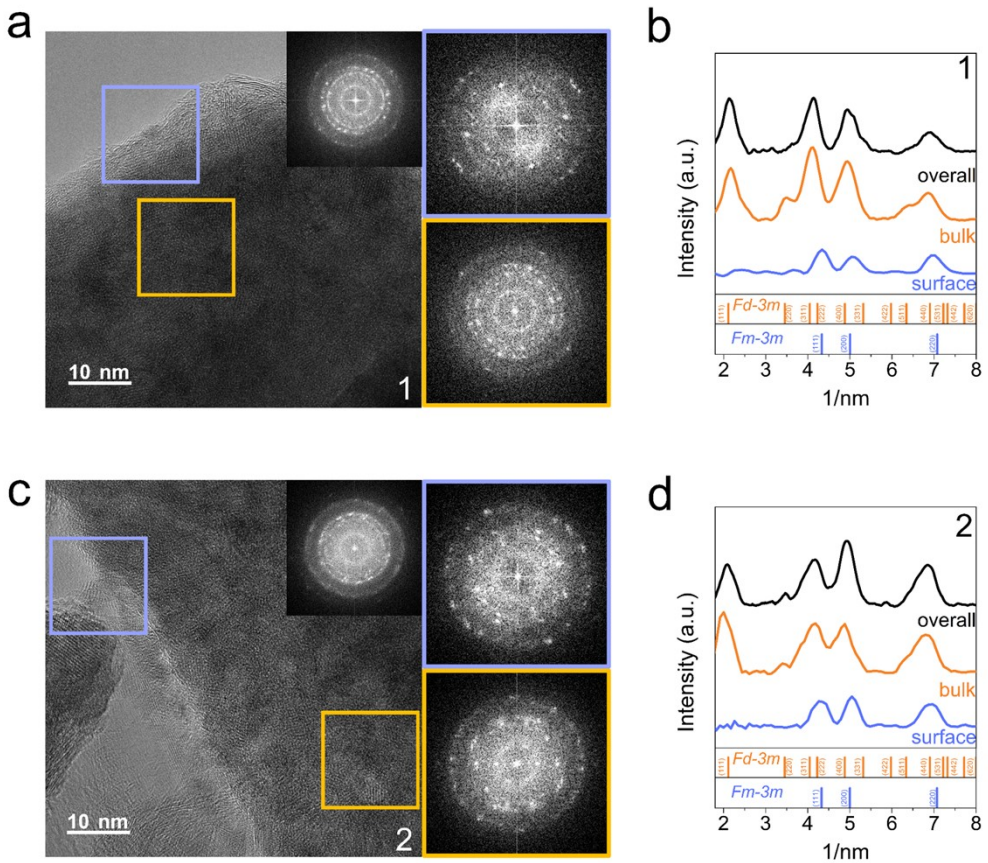


Fig. S19 (a, c) TEM images and FFT patterns of various regions of $\text{Li}_{1.26}\text{Mn}_{1.88}\text{O}_4$. The areas within the yellow and blue boxes at different local positions are dominated by spinel-like and DRX-like phases, respectively. (b,d) Azimuthal integration patterns of FFT for surface, bulk, and overall images in the TEM image of the same number.

Through TEM analysis, it was confirmed that similar to $\text{Li}_{1.33}\text{Mn}_2\text{O}_4$, $\text{Li}_{1.26}\text{Mn}_{1.88}\text{O}_4$ also contains an abundance of a DRX-like phase on its surface (Fig. S19). Differences in the structure can affect the EELS spectrum; hence, a shift in the spectra of the Mn $L_{3,2}$ -edge peak and the O K-edge peak was observed in the regions marked in the STEM-EELS image (Fig. S20). Similar to the spectral changes observed in the pristine state of $\text{Li}_{1.33}\text{Mn}_2\text{O}_4$, an energy shift between the surface and the bulk was also observed in $\text{Li}_{1.26}\text{Mn}_{1.88}\text{O}_4$.

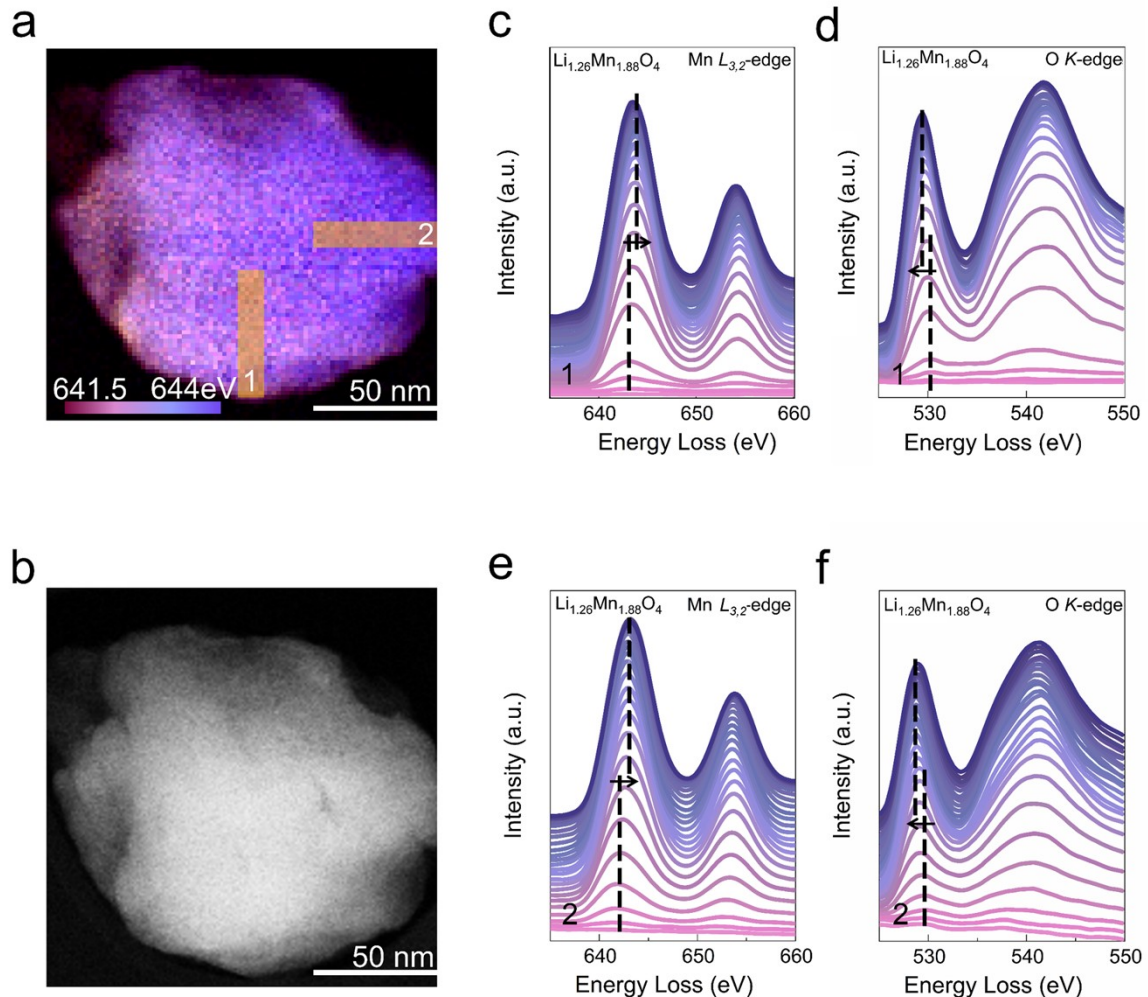


Fig. S20 a) STEM-EELS images of $\text{Li}_{1.26}\text{Mn}_{1.88}\text{O}_4$ for the energy distribution of the Mn $L_{3,2}$ -edge peak. (b) ADF TEM image of $\text{Li}_{1.26}\text{Mn}_{1.88}\text{O}_4$. EELS spectra of (c, e) Mn $L_{3,2}$ -edge peak and (d, f) O K-edge peak from the surface to bulk in the yellow box. (c,d) and (e,f) are spectra for yellow boxes no. 1 and no. 2, respectively.

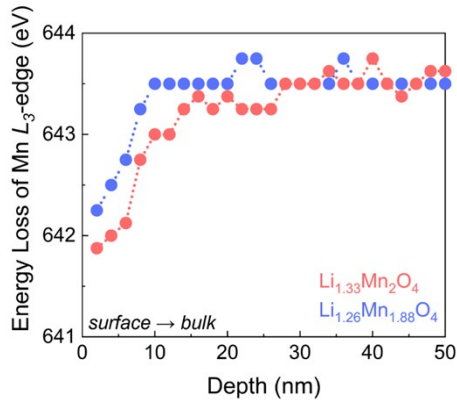


Fig. S21 Energy loss of Mn L_3 -edge according to depth in pristine state $\text{Li}_{1.33}\text{Mn}_2\text{O}_4$ and $\text{Li}_{1.26}\text{Mn}_{1.88}\text{O}_4$. The energy loss at each depth represents the average of the values measured in various local regions of the particle.

As depicted in Fig. S21, $\text{Li}_{1.26}\text{Mn}_{1.88}\text{O}_4$ exhibited an energy shift of 1.25 eV, which is smaller than the 1.75-eV shift observed in $\text{Li}_{1.33}\text{Mn}_2\text{O}_4$. Furthermore, $\text{Li}_{1.26}\text{Mn}_{1.88}\text{O}_4$ possessed a thinner surface thickness of the Mn reduced state (approximately 10 nm) compared with that of $\text{Li}_{1.33}\text{Mn}_2\text{O}_4$ (20 nm). This result may result from the DRX-like phase present on the surface being less extensive compared to $\text{Li}_{1.33}\text{Mn}_2\text{O}_4$. XRD refinement of Fig. S18 indicates that $\text{Li}_{1.26}\text{Mn}_{1.88}\text{O}_4$ consists of a spinel-like phase and a DRX-like phase in an 8:2 ratio, suggesting a higher proportion of the spinel-like phase compared to that in $\text{Li}_{1.33}\text{Mn}_2\text{O}_4$ (where these phases are present in a 7:3 ratio). This result implies that less DRX-like structures are present on the surface of $\text{Li}_{1.26}\text{Mn}_{1.88}\text{O}_4$.

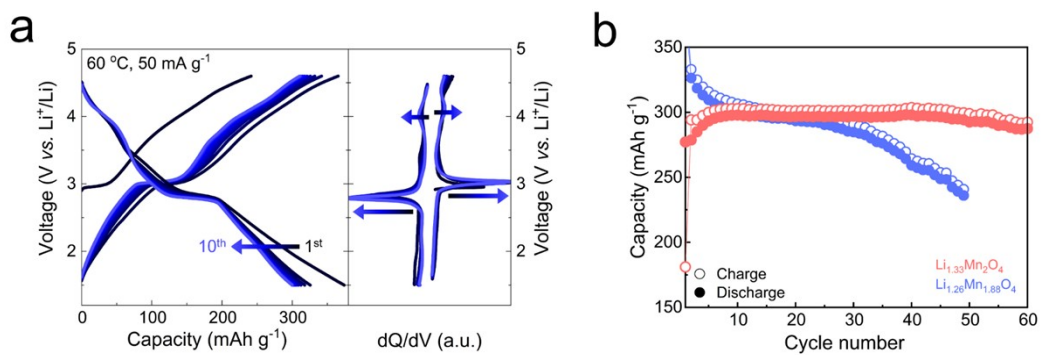


Fig. S22 (a) Electrochemical profile of $\text{Li}_{1.26}\text{Mn}_{1.88}\text{O}_4$ from 1st to 10th cycle (60 °C, 50 mA g⁻¹). (b) Comparison of capacity retention for $\text{Li}_{1.33}\text{Mn}_2\text{O}_4$ and $\text{Li}_{1.26}\text{Mn}_{1.88}\text{O}_4$.

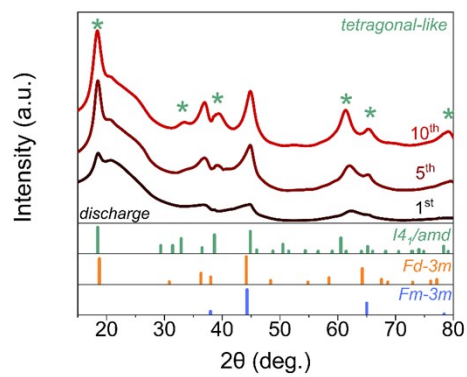


Fig. S23 *Ex-situ* XRD patterns of $\text{Li}_{1.26}\text{Mn}_{1.88}\text{O}_4$ at discharge state of various cycles

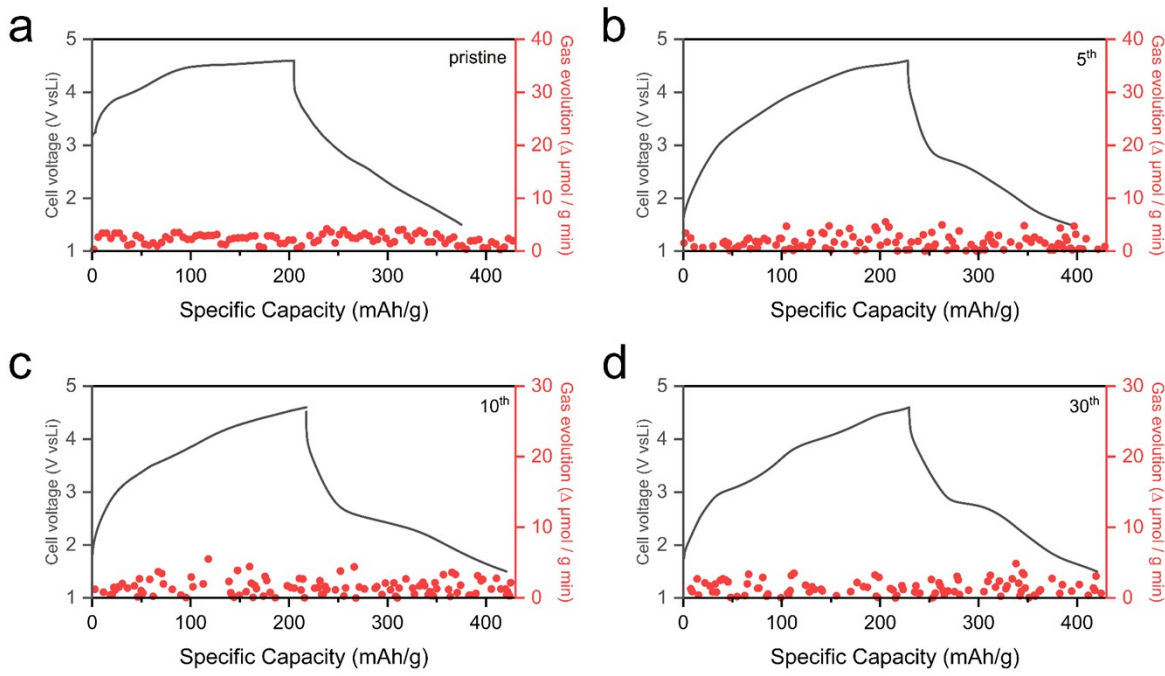


Fig. S24 DEMS results for $\text{Li}_{1.33}\text{Mn}_2\text{O}_4$ electrodes measured at various cycles: pristine electrode and 5th, 10th, and 30th cycles. Charging and discharging were performed at 20 mA g^{-1} at room temperature.

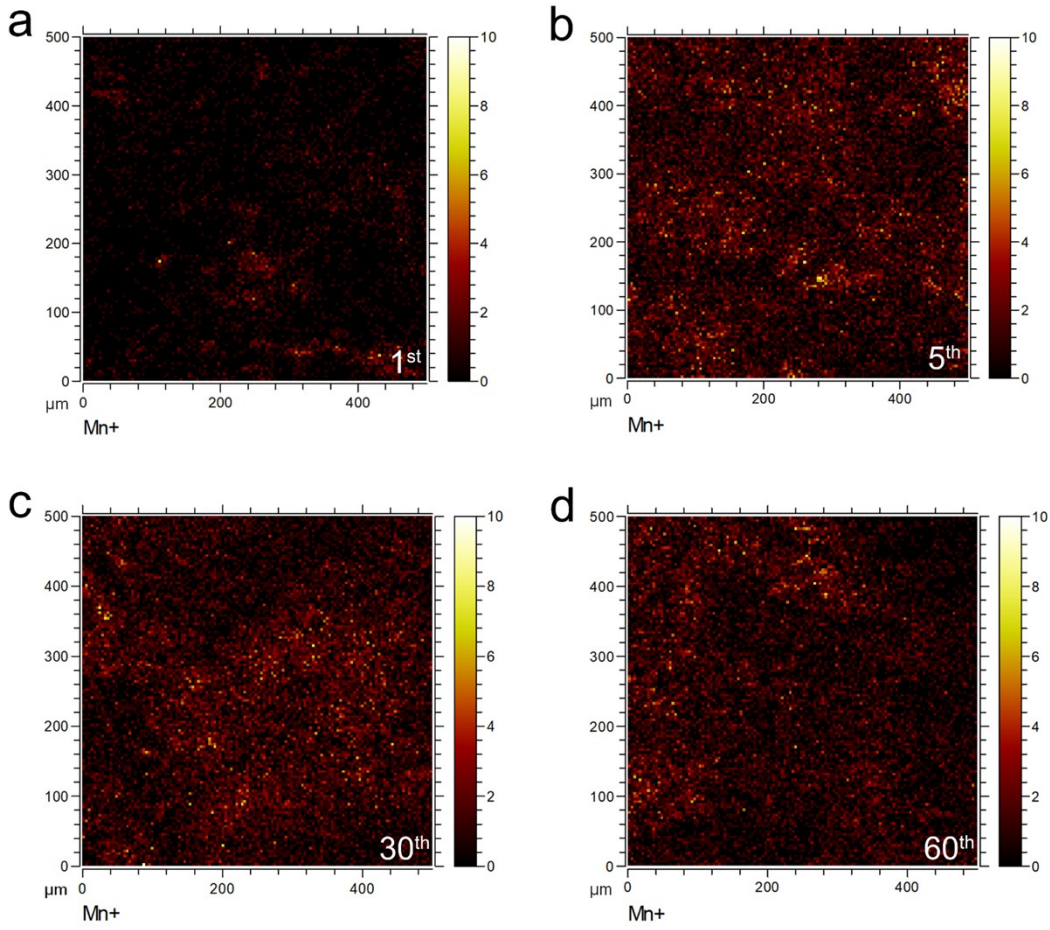


Fig. S25 TOF-SIMS images of Mn⁺ on Li anodes retrieved from half cells cycled with Li_{1.33}Mn₂O₄ as the cathode after (a) 1st, (b) 10th, (c) 30th, and (d) 60th cycle.

Dissolution of Mn ions is a critical factor affecting the performance of Mn-based cathode materials. Fig. S25 shows TOF-SIMS images of Mn ions retrieved on Li anode at various cycles of Li_{1.33}Mn₂O₄. The dissolution of Mn ions increases sharply during the first 5 cycles, followed by steady dissolution thereafter. However, as seen in Fig. S22b, the capacity of Li_{1.33}Mn₂O₄ increases up to the 10th cycle, remains stable until the 30th cycle, and then a slight decrease in capacity is observed. Similarly, for Li_{1.26}Mn_{1.88}O₄, the dissolution of Mn ions also increases sharply up to the initial 5 cycles, followed by continuous dissolution (Fig. S26). These results suggest that although Mn ion dissolution may contribute to capacity decline over the long term, it is not a major factor affecting the initial performance of Li_{1.33}Mn₂O₄ and Li_{1.26}Mn_{1.88}O₄.

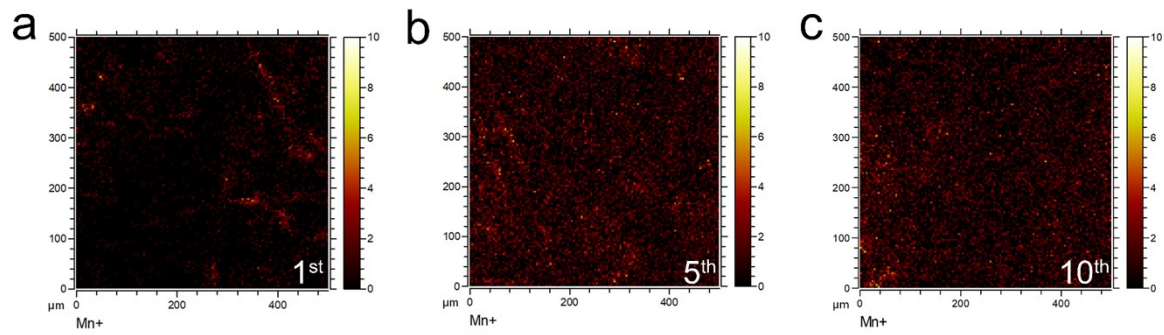


Fig. S26 TOF-SIMS images of Mn^+ in the Li anode from a half-cell cycled with $\text{Li}_{1.26}\text{Mn}_{1.88}\text{O}_4$ as the cathode after (a) the 1st, (b) 5th, and (c) 10th cycles.

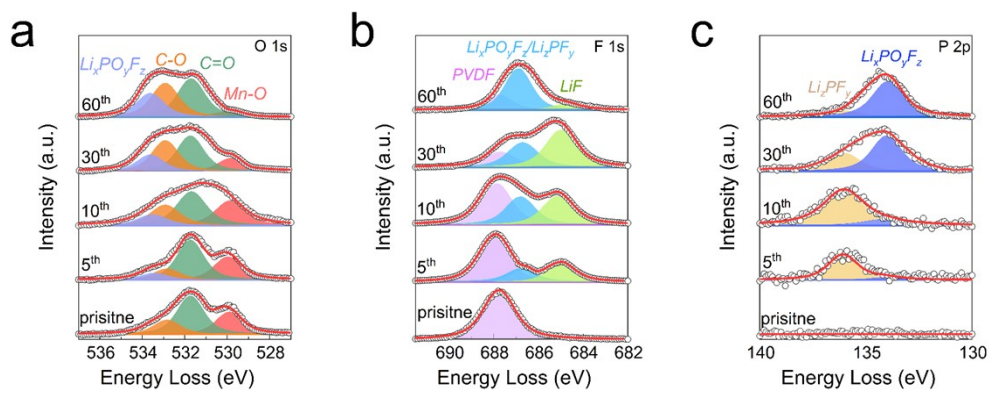


Fig. S27 (a) O 1s, (b) F 1s, and (c) P 2s XPS spectra of pristine $Li_{1.33}Mn_2O_4$ electrode and after 5th, 10th, 30th, and 60th cycle.

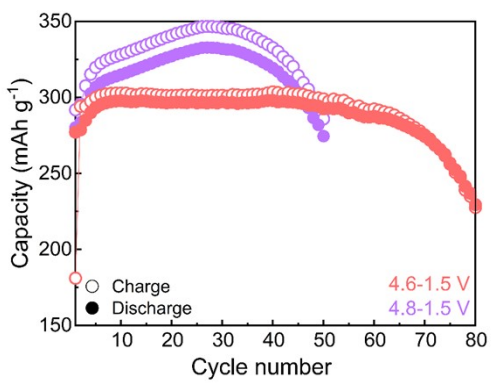


Fig. S28 Cycling performance of $\text{Li}_{1.33}\text{Mn}_2\text{O}_4$ in a high-voltage environment (4.8–1.5 V voltage range).

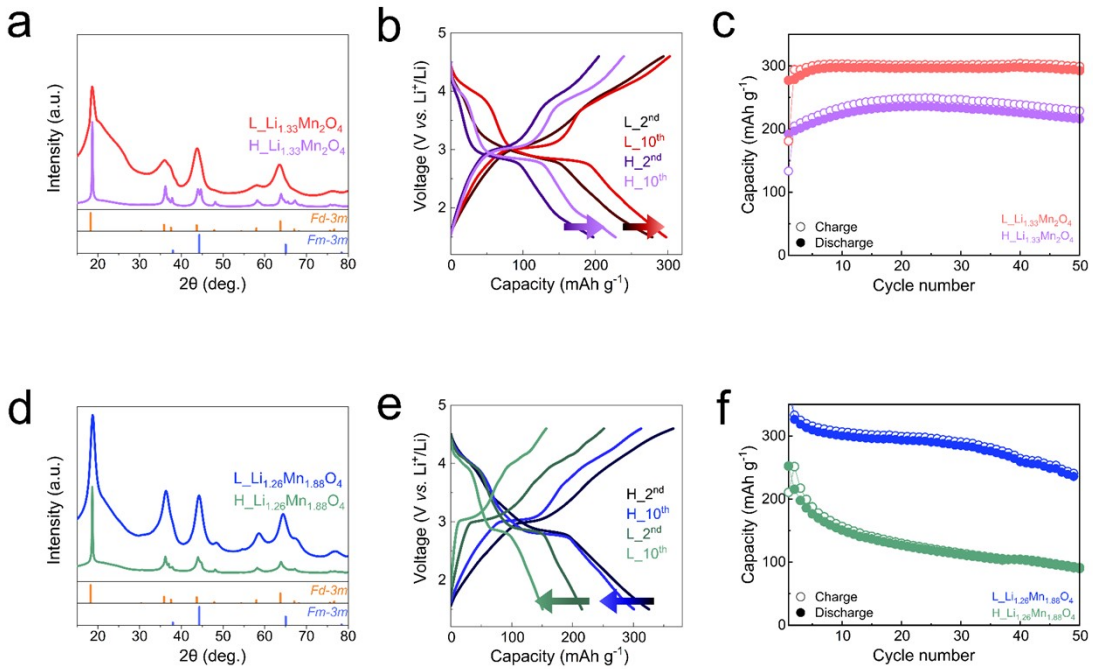


Fig. S29 (a,d)XRD patterns, (b,e)electrochemical profile, and (c,f)cycling performance of $\text{Li}_{1.33}\text{Mn}_2\text{O}_4$ and $\text{Li}_{1.26}\text{Mn}_{1.88}$ at various crystallinities.

To assess electrochemical performance at various crystallinities, we prepared $\text{H-Li}_{1.33}\text{Mn}_2\text{O}_4$ and $\text{H-Li}_{1.26}\text{Mn}_{1.88}\text{O}_4$ with relatively higher crystallinity by ball milling at 275 rpm, which is a lower energy compared to 530 rpm. Fig. S29a and d shows the XRD patterns for $\text{Li}_{1.33}\text{Mn}_2\text{O}_4$ and $\text{Li}_{1.26}\text{Mn}_{1.88}\text{O}_4$ synthesized at 530 rpm (L) and 275 rpm (H). The XRD patterns milled at 275 rpm are sharper than those at 530 rpm, indicating higher crystallinity. The $\text{H-Li}_{1.33}\text{Mn}_2\text{O}_4$ and $\text{H-Li}_{1.26}\text{Mn}_{1.88}\text{O}_4$, with higher crystallinity, show much lower capacities due to sluggish diffusion kinetics compared to those with lower crystallinity (Fig. S29b and e). In the case of $\text{Li}_{1.33}\text{Mn}_2\text{O}_4$, which has a higher ratio of DRX phase, the evolution of the 4 and 3 V plateaus is observed as cycles progress, regardless of crystallinity, suggesting a phase transition from DRX to spinel (Fig. 2). As seen in Fig. S29c, in $\text{H-Li}_{1.33}\text{Mn}_2\text{O}_4$, this transition period is extended due to sluggish diffusion kinetics. On the other hand, for $\text{Li}_{1.26}\text{Mn}_{1.88}\text{O}_4$, which has a lower ratio of the DRX phase, a decrease in capacity occurs regardless of crystallinity, and the capacity decrease in $\text{H-Li}_{1.26}\text{Mn}_{1.88}\text{O}_4$ occurs more quickly (Fig. S29f). Differences in electrochemical performance depending on crystallinity suggest that appropriate crystallinity can overcome slow kinetics and enhance material utilization.

Table S1 Crystallographic parameters of $\text{Li}_{1.33}\text{Mn}_2\text{O}_4$ obtained from Rietveld refinement.

Spinel-like phase	<i>Fd-3m</i>					fract.(%)	70.01
	a(Å)	b(Å)	c(Å)	$\alpha(^{\circ})$	$\beta(^{\circ})$	$\gamma(^{\circ})$	
Lattice parameters	8.1959	8.1959	8.1959	90	90	90	
	x	y	z	Occ.	B	Wyckoff symbol	
O1	0.2631	0.2631	0.2631	1.0000	0.558	32e	
Mn1	0.5000	0.5000	0.5000	0.8125	0.558	16d	
Mn2	0.0000	0.0000	0.0000	0.1875	0.558	16c	
Li1	0.1250	0.1250	0.1250	0.6130	0.558	8a	
Li2	0.0000	0.0000	0.0000	0.1280	0.558	16c	
Li3	0.5000	0.5000	0.5000	0.0920	0.558	16d	
DRX-like phase	<i>Fm-3m</i>					fract.(%)	29.79
	a(Å)	b(Å)	c(Å)	$\alpha(^{\circ})$	$\beta(^{\circ})$	$\gamma(^{\circ})$	
Lattice parameters	3.9998	3.9998	3.9998	90.0000	90	90	
	x	y	z	Occ.	B	Wyckoff symbol	
O1	0.5000	0.5000	0.5000	1.0000	0.5920	4b	
Mn1	0.0000	0.0000	0.0000	0.5000	0.5920	4a	
Li1	0.0000	0.0000	2.0000	0.4284	0.5920	4a	
Tetragonal-like phase	<i>I4₁/amd</i>					fract.(%)	0.20
	a(Å)	b(Å)	c(Å)	$\alpha(^{\circ})$	$\beta(^{\circ})$	$\gamma(^{\circ})$	
Lattice parameters	5.6500	5.6500	9.2200	90	90	90	
	x	y	z	Occ.	B	Wyckoff symbol	
O	0.0000	0.2686	0.3772	1.0000	0.5018	16h	
Mn1	0.7500	0.5000	0.3750	1.0000	0.5018	8c	
Li1	0.5000	0.7500	0.1250	1.0000	0.5018	8d	

Table S2 Crystallographic parameters of 5th discharge state obtained from Rietveld refinement performed on the ordered tetragonal phase.

Spinel-like phase		<i>Fd-3m</i>					44.48
		a(Å)	b(Å)	c(Å)	α(°)	β(°)	γ(°)
Lattice parameters		8.19100	8.19100	8.19100	90	90	90
		x	y	z	Occ.	B	Wyckoff symbol
O1		0.2631	0.2631	0.2631	1.0000	0.5942	32e
Mn1		0.5000	0.5000	0.5000	0.8351	0.5942	16d
Mn2		0.0000	0.0000	0.0000	0.1622	0.5942	16c
Li1		0.1250	0.1250	0.1250	0.2654	0.5942	8a
Li2		0.0000	0.0000	0.0000	0.6997	0.5942	16c
Li3		0.5000	0.5000	0.5000	0.1649	0.5942	16d

DRX-like phase		<i>Fm-3m</i>					16.00
		a(Å)	b(Å)	c(Å)	α(°)	β(°)	γ(°)
Lattice parameters		4.18703	4.18703	4.18703	90.0000	90	90
		x	y	z	Occ.	B	Wyckoff symbol
O1		0.5000	0.5000	0.5000	1.0000	0.5920	4b
Mn1		0.0000	0.0000	0.0000	0.5000	0.5920	4a
Li1		0.0000	0.0000	2.0000	0.5000	0.5920	4a

Tetragonal-like phase		<i>I4₁/amd</i>					39.52
		fract.(%)					
		a(Å)	b(Å)	c(Å)	α(°)	β(°)	γ(°)
Lattice parameters		5.68924	5.68924	9.09470	90	90	90
		x	y	z	Occ.	B	Wyckoff symbol
O		0.0000	0.2686	0.3772	1.0000	0.4921	16h
Mn1		0.7500	0.5000	0.3750	1.0000	0.4921	8c
Li1		0.5000	0.7500	0.1250	1.0000	0.4921	8d

Table S3 Crystallographic parameters of 1st, 5th, 10th, 30th, and 60th discharge states obtained from Rietveld refinement.

Refinement results for 1 st discharge						
Spinel-like phase	<i>Fd-3m</i>					fract.(%)
	a(Å)	b(Å)	c(Å)	α(°)	β(°)	γ(°)
Lattice parameters	8.19772	8.19772	8.19772	90	90	90
	x	y	z	Occ.	B	Wyckoff symbol
O1	0.2631	0.2631	0.2631	1.0000	0.5942	32e
Mn1	0.5000	0.5000	0.5000	0.8351	0.5942	16d
Mn2	0.0000	0.0000	0.0000	0.1622	0.5942	16c
Li1	0.1250	0.1250	0.1250	0.2654	0.5942	8a
Li2	0.0000	0.0000	0.0000	0.6997	0.5942	16c
Li3	0.5000	0.5000	0.5000	0.1649	0.5942	16d
DRX-like phase	<i>Fm-3m</i>					fract.(%)
	a(Å)	b(Å)	c(Å)	α(°)	β(°)	γ(°)
Lattice parameters	4.18703	4.18703	4.18703	90.0000	90	90
	x	y	z	Occ.	B	Wyckoff symbol
O1	0.5000	0.5000	0.5000	1.0000	0.5201	4b
Mn1	0.0000	0.0000	0.0000	0.5000	0.5201	4a
Li1	0.0000	0.0000	2.0000	0.5000	0.5201	4a
Tetragonal-like phase	<i>I4/amd</i>					fract.(%)
	a(Å)	b(Å)	c(Å)	α(°)	β(°)	γ(°)
Lattice parameters	5.6932575	5.6932579	9.002119	90	90	90
	x	y	z	Occ.	B	Wyckoff symbol
O	0.0000	0.2686	0.3772	1.0000	0.5841	16h
Mn1	0.5000	0.7500	0.1250	0.3998	0.5841	8d
Mn2	0.7500	0.5000	0.3750	0.6002	0.5841	8c
Li1	0.5000	0.7500	0.1250	0.6002	0.5841	8d
Li2	0.7500	0.5000	0.3750	0.3998	0.5841	8c
Refinement results for 5 th discharge						
Spinel-like phase	<i>Fd-3m</i>					fract.(%)
	a(Å)	b(Å)	c(Å)	α(°)	β(°)	γ(°)
Lattice parameters	8.19100	8.19100	8.19100	90	90	90
	x	y	z	Occ.	B	Wyckoff symbol
O1	0.2631	0.2631	0.2631	1.0000	0.5942	32e
Mn1	0.5000	0.5000	0.5000	0.8351	0.5942	16d
Mn2	0.0000	0.0000	0.0000	0.1622	0.5942	16c
Li1	0.1250	0.1250	0.1250	0.2654	0.5942	8a
Li2	0.0000	0.0000	0.0000	0.6997	0.5942	16c
Li3	0.5000	0.5000	0.5000	0.1649	0.5942	16d
DRX-like phase	<i>Fm-3m</i>					fract.(%)
						16.00

	a(Å)	b(Å)	c(Å)	$\alpha(^{\circ})$	$\beta(^{\circ})$	$\gamma(^{\circ})$
Lattice parameters	4.18703	4.18703	4.18703	90.0000	90	90
	x	y	z	Occ.	B	Wyckoff symbol
O1	0.5000	0.5000	0.5000	1.0000	0.5201	4b
Mn1	0.0000	0.0000	0.0000	0.5000	0.5201	4a
Li1	0.0000	0.0000	2.0000	0.5000	0.5201	4a

Tetragonal-like phase	<i>I4₁/amd</i>		fract.(%)	39.52		
	a(Å)	b(Å)	c(Å)	$\alpha(^{\circ})$	$\beta(^{\circ})$	$\gamma(^{\circ})$
Lattice parameters	5.68924	5.68924	9.09470	90	90	90
	x	y	z	Occ.	B	Wyckoff symbol
O	0.0000	0.2686	0.3772	1.0000	0.4921	16h
Mn1	0.5000	0.7500	0.1250	0.3170	0.4921	8d
Mn2	0.7500	0.5000	0.3750	0.6979	0.4921	8c
Li1	0.5000	0.7500	0.1250	0.6979	0.4921	8d
Li2	0.7500	0.5000	0.3750	0.3170	0.4921	8c

Refinement results for the 10 th discharge						
Spinel-like phase	<i>Fd-3m</i>			fract.(%)	36.99	
	a(Å)	b(Å)	c(Å)	$\alpha(^{\circ})$	$\beta(^{\circ})$	$\gamma(^{\circ})$
Lattice parameters	8.18992	8.18992	8.18992	90	90	90
	x	y	z	Occ.	B	Wyckoff symbol
O1	0.2631	0.2631	0.2631	1.0000	0.5942	32e
Mn1	0.5000	0.5000	0.5000	0.8351	0.5942	16d
Mn2	0.0000	0.0000	0.0000	0.1622	0.5942	16c
Li1	0.1250	0.1250	0.1250	0.2654	0.5942	8a
Li2	0.0000	0.0000	0.0000	0.6997	0.5942	16c
Li3	0.5000	0.5000	0.5000	0.1649	0.5942	16d
DRX-like phase	<i>Fm-3m</i>			fract.(%)	11.85	
	a(Å)	b(Å)	c(Å)	$\alpha(^{\circ})$	$\beta(^{\circ})$	$\gamma(^{\circ})$
Lattice parameters	4.19908	4.19908	4.19908	90.0000	90	90
	x	y	z	Occ.	B	Wyckoff symbol
O1	0.5000	0.5000	0.5000	1.0000	0.5201	4b
Mn1	0.0000	0.0000	0.0000	0.5000	0.5201	4a
Li1	0.0000	0.0000	2.0000	0.5000	0.5201	4a
Tetragonal-like phase	<i>I4₁/amd</i>			fract.(%)	51.16	
	a(Å)	b(Å)	c(Å)	$\alpha(^{\circ})$	$\beta(^{\circ})$	$\gamma(^{\circ})$
Lattice parameters	5.67895	5.67895	9.12344	90	90	90
	x	y	z	Occ.	B	Wyckoff symbol
O	0.0000	0.2686	0.3772	1.0000	0.5991	16h
Mn1	0.5000	0.7500	0.1250	0.3050	0.5991	8d
Mn2	0.7500	0.5000	0.3750	0.6950	0.5991	8c

Li1	0.5000	0.7500	0.1250	0.6950	0.5991	8d
Li2	0.7500	0.5000	0.3750	0.3050	0.5991	8c

Refinement results for 30 th discharge						
Spinel-like phase	<i>Fd-3m</i>					fract.(%)
	a(Å)	b(Å)	c(Å)	$\alpha(^{\circ})$	$\beta(^{\circ})$	$\gamma(^{\circ})$
Lattice parameters	8.19510	8.19510	8.19510	90	90	90
	x	y	z	Occ.	B	Wyckoff symbol
O1	0.2631	0.2631	0.2631	1.0000	0.5942	32e
Mn1	0.5000	0.5000	0.5000	0.8351	0.5942	16d
Mn2	0.0000	0.0000	0.0000	0.1622	0.5942	16c
Li1	0.1250	0.1250	0.1250	0.2654	0.5942	8a
Li2	0.0000	0.0000	0.0000	0.6997	0.5942	16c
Li3	0.5000	0.5000	0.5000	0.1649	0.5942	16d
DRX-like phase	<i>Fm-3m</i>					fract.(%)
	a(Å)	b(Å)	c(Å)	$\alpha(^{\circ})$	$\beta(^{\circ})$	$\gamma(^{\circ})$
Lattice parameters	4.20704	4.20704	4.20704	90.0000	90	90
	x	y	z	Occ.	B	Wyckoff symbol
O1	0.5000	0.5000	0.5000	1.0000	0.5201	4b
Mn1	0.0000	0.0000	0.0000	0.5000	0.5201	4a
Li1	0.0000	0.0000	2.0000	0.5000	0.5201	4a
Tetragonal-like phase	<i>I4₁/amd</i>					fract.(%)
	a(Å)	b(Å)	c(Å)	$\alpha(^{\circ})$	$\beta(^{\circ})$	$\gamma(^{\circ})$
Lattice parameters	5.66375	5.66375	9.16675	90	90	90
	x	y	z	Occ.	B	Wyckoff symbol
O	0.0000	0.2686	0.3772	1.0000	0.5737	16h
Mn1	0.5000	0.7500	0.1250	0.1832	0.5737	8d
Mn2	0.7500	0.5000	0.3750	0.8168	0.5737	8c
Li1	0.5000	0.7500	0.1250	0.8168	0.5737	8d
Li2	0.7500	0.5000	0.3750	0.1832	0.5737	8c

Refinement results for the 60 th discharge						
Spinel-like phase	<i>Fd-3m</i>					fract.(%)
	a(Å)	b(Å)	c(Å)	$\alpha(^{\circ})$	$\beta(^{\circ})$	$\gamma(^{\circ})$
Lattice parameters	8.20715	8.20715	8.20715	90	90	90
	x	y	z	Occ.	B	Wyckoff symbol
O1	0.2631	0.2631	0.2631	1.0000	0.5942	32e
Mn1	0.5000	0.5000	0.5000	0.8351	0.5942	16d
Mn2	0.0000	0.0000	0.0000	0.1622	0.5942	16c
Li1	0.1250	0.1250	0.1250	0.2654	0.5942	8a
Li2	0.0000	0.0000	0.0000	0.6997	0.5942	16c

Li3	0.5000	0.5000	0.5000	0.1649	0.5942	16d
DRX-like phase	<i>Fm-3m</i>				fract.(%)	0.06
	a(Å)	b(Å)	c(Å)	$\alpha(^{\circ})$	$\beta(^{\circ})$	$\gamma(^{\circ})$
Lattice parameters	5.19791	5.19791	5.19791	90.0000	90	90
	x	y	z	Occ.	B	Wyckoff symbol
O1	0.5000	0.5000	0.5000	1.0000	0.5201	4b
Mn1	0.0000	0.0000	0.0000	0.5000	0.5201	4a
Li1	0.0000	0.0000	2.0000	0.5000	0.5201	4a
Tetragonal-like phase	<i>I4/amd</i>				fract.(%)	88.80
	a(Å)	b(Å)	c(Å)	$\alpha(^{\circ})$	$\beta(^{\circ})$	$\gamma(^{\circ})$
Lattice parameters	5.66826	5.66826	9.18253	90	90	90
	x	y	z	Occ.	B	Wyckoff symbol
O	0.0000	0.2686	0.3772	1.0000	0.5403	16h
Mn1	0.5000	0.7500	0.1250	0.15308	0.5403	8d
Mn2	0.7500	0.5000	0.3750	0.84692	0.5403	8c
Li1	0.5000	0.7500	0.1250	0.84692	0.5403	8d
Li2	0.7500	0.5000	0.3750	0.15308	0.5403	8c

Table S4 Crystallographic parameters of $\text{Li}_{1.26}\text{Mn}_{1.88}\text{O}_4$ obtained from Rietveld refinement.

Spinel-like phase	<i>Fd-3m</i>					fract.(%)	80.87
	a(Å)	b(Å)	c(Å)	$\alpha(^{\circ})$	$\beta(^{\circ})$	$\gamma(^{\circ})$	
Lattice parameters	8.19757	8.19757	8.19757	90	90	90	
	x	y	z	Occ.	B	Wyckoff symbol	
O1	0.2631	0.2631	0.2631	1.0000	0.558	32e	
Mn1	0.5000	0.5000	0.5000	0.8125	0.558	16d	
Mn2	0.0000	0.0000	0.0000	0.1875	0.558	16c	
Li1	0.1250	0.1250	0.1250	0.6320	0.558	8a	
Li2	0.0000	0.0000	0.0000	0.1280	0.558	16c	
Li3	0.5000	0.5000	0.5000	0.0820	0.558	16d	
DRX-like phase	<i>Fm-3m</i>					fract.(%)	19.13
	a(Å)	b(Å)	c(Å)	$\alpha(^{\circ})$	$\beta(^{\circ})$	$\gamma(^{\circ})$	
Lattice parameters	4.00180	4.00180	4.00180	90.0000	90	90	
	X	y	z	Occ.	B	Wyckoff symbol	
O1	0.5000	0.5000	0.5000	1.0000	0.5920	4b	
Mn1	0.0000	0.0000	0.0000	0.5000	0.5920	4a	
Li1	0.0000	0.0000	2.0000	0.3330	0.5920	4a	
Tetragonal-like phase	<i>I4₁/amd</i>					fract.(%)	0
	a(Å)	b(Å)	c(Å)	$\alpha(^{\circ})$	$\beta(^{\circ})$	$\gamma(^{\circ})$	
Lattice parameters	5.6500	5.6500	9.2200	90	90	90	
	x	y	z	Occ.	B	Wyckoff symbol	
O	0.0000	0.2686	0.3772	1.0000	0.5018	16h	
Mn1	0.5000	0.7500	0.1250	0.0000	0.5018	8d	
Mn2	0.7500	0.5000	0.3750	1.0000	0.5018	8c	
Li1	0.5000	0.7500	0.1250	1.0000	0.5018	8d	
Li2	0.7500	0.5000	0.3750	0.0000	0.5018	8c	